ARMY RESEARCH LABORATORY

Development of Geomaterial Parameters for Numerical Simulations Using the Holmquist-Johnson-Cook Constitutive Model for Concrete

by Christopher S. Meyer

ARL-TR-5556   **June 2011**

NOTICES

Disclaimers

Army Research Laboratory

Aberdeen Proving Ground, MD 21005-5069

ARL-TR-5556 June 2011

Development of Geomaterial Parameters for Numerical Simulations Using the Holmquist-Johnson-Cook Constitutive Model for Concrete

Christopher S. Meyer
Weapons and Materials Research Directorate, ARL

Approved for public release; distribution unlimited.

REPORT DOCUMENTATION PAGE			*Form Approved* *OMB No. 0704-0188*
Public reporting burden for this collection of information is estimated to average 1 hour per response, including the time for reviewing instructions, searching existing data sources, gathering and maintaining the data needed, and completing and reviewing the collection information. Send comments regarding this burden estimate or any other aspect of this collection of information, including suggestions for reducing the burden, to Department of Defense, Washington Headquarters Services, Directorate for Information Operations and Reports (0704-0188), 1215 Jefferson Davis Highway, Suite 1204, Arlington, VA 22202-4302. Respondents should be aware that notwithstanding any other provision of law, no person shall be subject to any penalty for failing to comply with a collection of information if it does not display a currently valid OMB control number. **PLEASE DO NOT RETURN YOUR FORM TO THE ABOVE ADDRESS.**			

1. REPORT DATE *(DD-MM-YYYY)* June 2011	2. REPORT TYPE Final		3. DATES COVERED *(From - To)* 06-09-2009–03-14-2011
4. TITLE AND SUBTITLE Development of Geomaterial Parameters for Numerical Simulations Using the Holmquist-Johnson-Cook Constitutive Model for Concrete			5a. CONTRACT NUMBER
			5b. GRANT NUMBER
			5c. PROGRAM ELEMENT NUMBER
6. AUTHOR(S) Christopher S. Meyer			5d. PROJECT NUMBER
			5e. TASK NUMBER
			5f. WORK UNIT NUMBER
7. PERFORMING ORGANIZATION NAME(S) AND ADDRESS(ES) U.S. Army Research Laboratory ATTN: RDRL-WML-H Aberdeen Proving Ground, MD 21005-5069			8. PERFORMING ORGANIZATION REPORT NUMBER ARL-TR-5556
9. SPONSORING/MONITORING AGENCY NAME(S) AND ADDRESS(ES)			10. SPONSOR/MONITOR'S ACRONYM(S)
			11. SPONSOR/MONITOR'S REPORT NUMBER(S)

12. DISTRIBUTION/AVAILABILITY STATEMENT
Approved for public release; distribution unlimited.

13. SUPPLEMENTARY NOTES

14. ABSTRACT
Numerical simulation of brick and mortar masonry in the literature has been performed using homogenized material properties; however, heterogeneous material properties for brick and mortar for a constitutive model built into hydrocodes have been unavailable. The Holmquist-Johnson-Cook (HJC) constitutive model for concrete captures pressure and strain-rate-dependent strength behavior and void crushing damage behavior of porous materials reasonably well, is readily available in many hydrocodes, and is commonly used to simulate high-velocity penetration of concrete. This report describes the development of the brick and mortar material parameters for the HJC material model—including exploration of the materials' strength, damage, and pressure behavior—from available static and dynamic test data for brick, two types of mortar, and adobe. The report also presents sample numerical simulations, using the material parameters developed, and compares the resulting material behavior to mechanical test data.

15. SUBJECT TERMS
Geomaterials, brick, computer simulation, dynamic behavior

16. SECURITY CLASSIFICATION OF:			17. LIMITATION OF ABSTRACT	18. NUMBER OF PAGES	19a. NAME OF RESPONSIBLE PERSON Christopher S. Meyer
a. REPORT Unclassified	b. ABSTRACT Unclassified	c. THIS PAGE Unclassified	UU	24	19b. TELEPHONE NUMBER *(Include area code)* (410) 278-3803

Standard Form 298 (Rev. 8/98)
Prescribed by ANSI Std. Z39.18

Contents

List of Figures

List of Tables

1. Introduction

The U.S. Army's interest in urban operations has led to efforts at the U.S. Army Research Laboratory to develop an initial set of material model parameters to enable physics-based penetration simulations of high-fidelity brick and mortar masonry wall models. These material model parameters take advantage of the Holmquist-Johnson-Cook (HJC) model for concrete (*1*).

A search of publically released literature turned up little involving modeling and simulation of weapon effects against brick and mortar targets. While dynamic material properties for concrete are well characterized, the dynamic material properties of brick and mortar are in the early stages of investigation. Research involving material properties for masonry for use in numerical simulations has concentrated on homogenized material properties and material models, which smear the mortar and brick together into a single material rather than discrete, heterogeneous brick and mortar materials (*2, 3*). Research involving numerical simulation of masonry walls has concentrated on the structural response of the walls to blast loading (*4, 5*). According to Shieh-Beygi and Pietruszczak, "…analysis of large masonry structures should best be conducted at a macro-level… described as a continuum whose average properties are identified at the level of constituents taking into account their geometric arrangement (*6*)." The homogenized material property methods described in these sources are effective for macroscopic behavior of masonry walls in response to shear loads as from earthquakes or in response to blast loading as from weapon effects. But the behavior of brick and mortar masonry in response to high-velocity penetration requires heterogeneous brick and mortar models and material parameters to better explore the shock interaction across multiple layers of materials with dissimilar sound speeds, densities, and pressure-dependent strength behavior.

Shieh-Beygi and Pietruszczak provide a brief review of homogenized constitutive models for brick and mortar masonry and then develop their own mesoscale constitutive model (*6*). Development of a constitutive material model for brick and mortar is beyond the scope of this work, which instead developed material parameters for the existing HJC constitutive model for concrete. Considering the void-collapse strain behavior of geomaterials, it is assumed that the HJC concrete model—widely available in Lagrangian and Eulerian simulation codes and shown to produce reasonable residual velocity results in high-velocity concrete penetration simulations when compared with experiment (*7*)—captures the void-crushing damage, strain-rate, and pressure-dependent strength properties of brick and mortar sufficiently well to simulate physics-based penetration of these materials. This work developed complete sets of HJC constitutive model material parameters for grade SW brick and type S mortar from mechanical characterization data provided by the U.S. Army Corps of Engineers, Engineer Research and Development Center (ERDC) (*8, 9*).

2. Development of Material Parameters

2.1 Strength

As described in Holmquist et al. (*1*), the constitutive equation 1 expresses the pressure- and strain-rate-dependent strength of the subject material; equation 1 states that the material's yield strength, when the material is confined, will increase with increasing pressure and with increasing strain rate. The constants *A*, *B*, *C*, and *N* are material parameters determined by fitting the model to test data, *D* is scalar damage, *P** is normalized pressure, and σ^* is the normalized compressive yield strength of the material. Strength and pressure are normalized by dividing by the unconfined compressive strength, *f'c,* of the material, which was determined from unconfined, axial compression mechanical test data provided by ERDC (*8, 9*). Strain rate is made dimensionless by dividing the actual strain rate, $\dot{\varepsilon}$, by a reference strain rate, $\dot{\varepsilon}_o$, typically 1.0 s^{-1}. Damage is a value from 0 to 1 that describes the accumulation of damage as a percentage of the full cohesive strength that the material possesses such that at *D* = 0 the material is undamaged and exhibits its full strength, but at *D* = 1 the material is fully damaged and retains the least confined shear strength. The first term of the constitutive equation 1 describes the pressure-dependent strength behavior of the subject materials, the second term describes the strain rate effects, and a third term, which is not shown here, describes the temperature-dependent strength of the material; temperature effects are not explored in the present work.

$$\sigma^* = \left(A \cdot (1 - D) + B \cdot P^{*N} \right) \left(1 + C \cdot \ln \left(\frac{\dot{\varepsilon}}{\dot{\varepsilon}_o} \right) \right) \tag{1}$$

The pressure-dependent strength behaviors of brick and mortar, as expressed by equation 1, were fit to mechanical test data from Williams et al. (*8, 9*). These data included uniaxial strain (UX) stress-strain and pressure-strength data, found by loading confined cylindrical samples of material in the axial direction, and triaxial compression (TXC) pressure-strength data, found by loading cylindrical samples in hydrostatic compression up to predefined confining pressures and then loading samples axially while holding radial confining pressure constant. The strength fits are shown in figures 1 and 2 for grade SW brick and type S mortar, respectively.

To determine the material strength constants, the cohesive strength constant, *A*, and the strain rate coefficient, *C*, were found, and then the remaining strength constants, *B* and *N*, were obtained by fitting equation 1 to UX test data. The cohesive strength constant, *A*, relates undamaged material strength to completely fractured material strength, at constant pressure, and was calculated from TXC failure data and UX pressure-stress data, both tested at a strain rate of approximately 10^{-5} s^{-1}, and then *A* was normalized to the reference strain rate, 1.0 s^{-1}, by scaling up by means of the dynamic increase factors (DIF) presented for brick and for mortar by Hao and Tarasov (*10*). The grade SW brick cohesive strength constant was determined at a pressure

of approximately 75 MPa, which corresponds to a normalized pressure of about $P^* = 1$; the type S mortar cohesive strength constant was determined at a pressure of approximately 20 MPa, which corresponds to a normalized pressure of about $P^* = 1.6$.
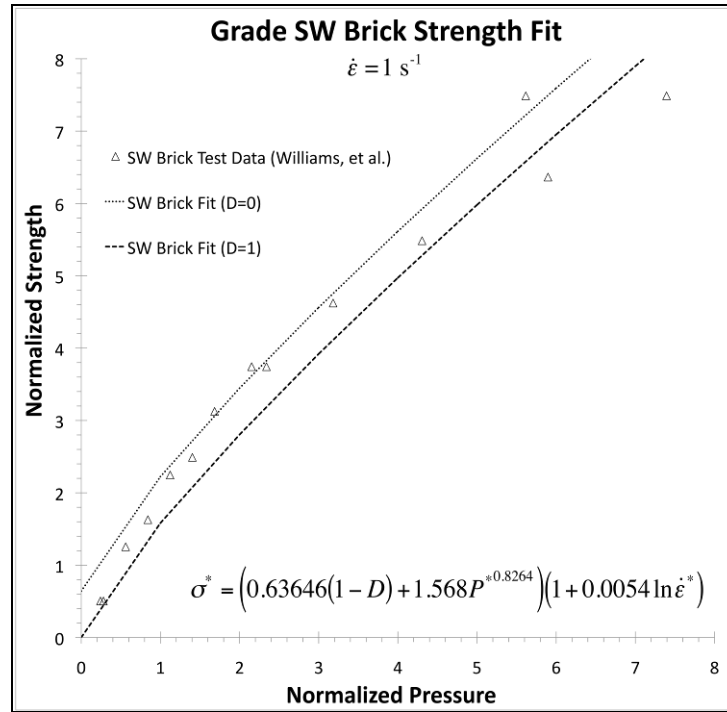

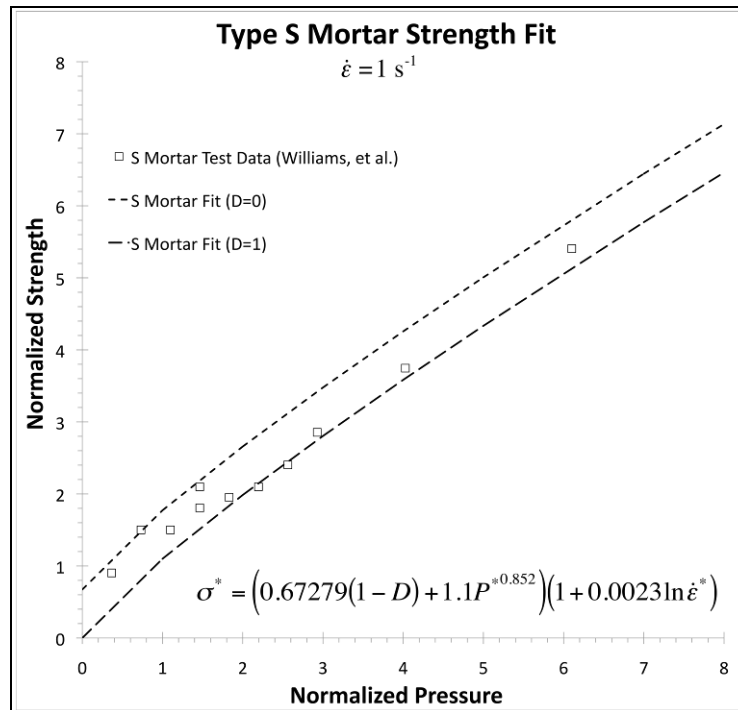Figure 1. HJC material model strength fit for grade SW brick.

Figure 2. HJC material model strength fit for type S mortar.

The strain rate coefficient, *C*, was found for brick from strain-rate-dependent strength data from Hao and Tarasov (*10*); strain rate coefficient was found for mortar from strain-rate-dependent strength data from Grote et al. (*11*). Material strength—normalized to the average quasi-static unconfined compressive strength of the tested materials, 44.83 MPa for brick and 46 MPa for mortar—versus strain rate was plotted for brick and for mortar; the slopes of linear fits through the two data sets were used for the strain rate coefficient of the respective materials.

Once *A* and *C* were determined, the pressure hardening constant, *B*, and the pressure hardening exponent, *N*, were fit to UX data using equation 1.

2.2   Damage

Damage is defined as the accumulation of equivalent plastic strain, $\Delta\varepsilon_p$—strain due to deformation and fracture—and plastic volumetric strain, $\Delta\mu_p$—strain due to crushing and void collapse—over each time step; damage is expressed as equation 2 (*1, 12*). The model calculates damage by summing the equivalent plastic strain and plastic volumetric strain and dividing the sum by the plastic strain to fracture under a constant pressure. The plastic strain to fracture under constant pressure may be found from whichever is greater, EFMIN or plastic strain to fracture found from equation 3. Thus, EFMIN provides for a minimum plastic strain value that will cause the material to fracture; since cyclic unconfined compressive failure data is not available for these materials, the default value of 0.01 is used in this work for all materials. Plastic strain to fracture is determined by the model from two damage constants, *D1* and *D2*, and from the normalized pressure, P^*, and normalized tensile strength, T^*. The tensile strength constant for each material is found from direct pull test data. *D1* was found from unconfined compression test data, and *D2* was chosen to be 1.0, which assumes that plastic fracture strain increases linearly with increasing pressure. Damage relationships are shown in figure 3. Further study of the fracture behavior of these materials is necessary to fully understand the effect damage has on strength, particularly the linear assumption, but fracture data are presently unavailable for brick and for mortar.

$$D = \sum \frac{\Delta\varepsilon_p + \Delta\mu_p}{\varepsilon_f} \tag{2}$$

$$\varepsilon_f = D1(P^* + T^*)^{D2} \tag{3}$$

Damage accumulates in geomaterials under load as the material fractures (the accumulation of equivalent plastic strain) and as the voids in the porous material compress and collapse (the accumulation of plastic volumetric strain). The majority of damage is accumulated through fracturing of the material with crushing of the material accounting for a small amount of the total damage. As damage accumulates, the scalar damage parameter from equations 1 and 2, *D*, will approach a value of 1 (or 100%); as damage approaches 100%, the normalized cohesive strength term, *A*, from equation 1 approaches zero, which is a loss of shear strength of the material.
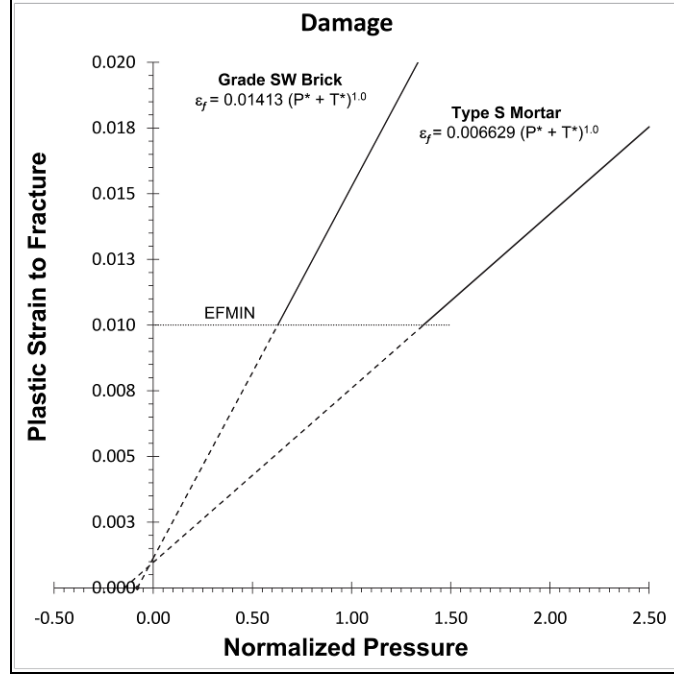
Figure 3. HJC material model damage fit for brick and mortar.

2.3 Pressure

Holmquist et al. (*1*) describes the materials' hydrostatic pressure response to volumetric strain in three distinct regions. The material behaves differently as pressure increases. At low pressure, less than crush pressure, P_{crush}, the material undergoes reversible, elastic deformation. The model predicts this elastic behavior with a simple linear relationship controlled by the user's input of the parameters P_{crush} and μ_{crush}. Elastic bulk modulus, K_e, is calculated by the model as the crush pressure divided by the crush volumetric strain: $K_e = P_{crush}/\mu_{crush}$. This region of elastic material behavior is known as Region I. In Region I, the model, according to a simple linear relationship, predicts pressure as the applied volumetric strain multiplied by the elastic bulk modulus. Figures 4 and 5 illustrate the pressure-volume behavior of grade SW brick and type S mortar, respectively; Region I is shown as insets in these figures. For brittle geomaterials, the elastic region of behavior is very small. P_{crush} and μ_{crush} were determined by fitting to hydrostatic compression (HC) and UX mechanical test data as shown in figures 4 and 5.
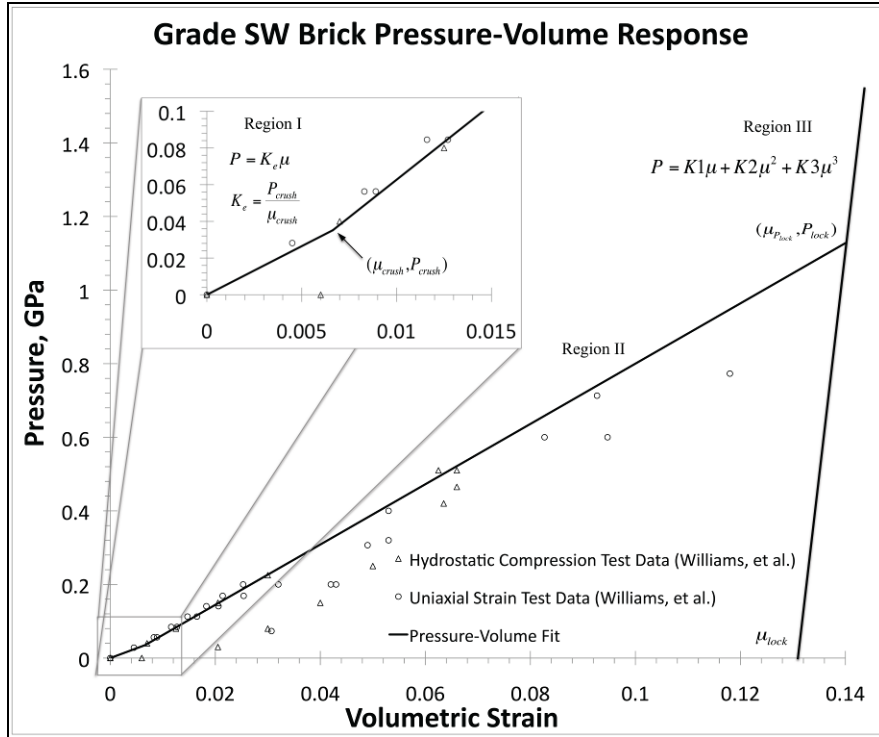
5

Grade SW Brick Pressure-Volume Response

Region I
$P = K_e \mu$
$K_e = \dfrac{P_{crush}}{\mu_{crush}}$
(μ_{crush}, P_{crush})

Region III
$P = K1\mu + K2\mu^2 + K3\mu^3$

$(\mu_{P_{lock}}, P_{lock})$

Region II

$\triangle$ Hydrostatic Compression Test Data (Williams, et al.)
$\circ$ Uniaxial Strain Test Data (Williams, et al.)
— Pressure-Volume Fit

μ_{lock}

Pressure, GPa

Volumetric Strain

Figure 4. HJC material model pressure-volume fit for grade SW brick.

Type S Mortar Pressure-Volume Response

$\triangle$ Hydrostatic Compression Test Data (Williams, et al.)
$\square$ Uniaxial Strain Constant Volume Test Data (Williams, et al.)
$\circ$ Uniaxial Strain Test Data (Williams, et al.)
— Pressure-Volume Fit

Region I
$P = K_e \mu$
(μ_{crush}, P_{crush}) $K_e = \dfrac{P_{crush}}{\mu_{crush}}$

Region III
$P = K1\mu + K2\mu^2 + K3\mu^3$

$(\mu_{P_{lock}}, P_{lock})$

Region II

μ_{lock}
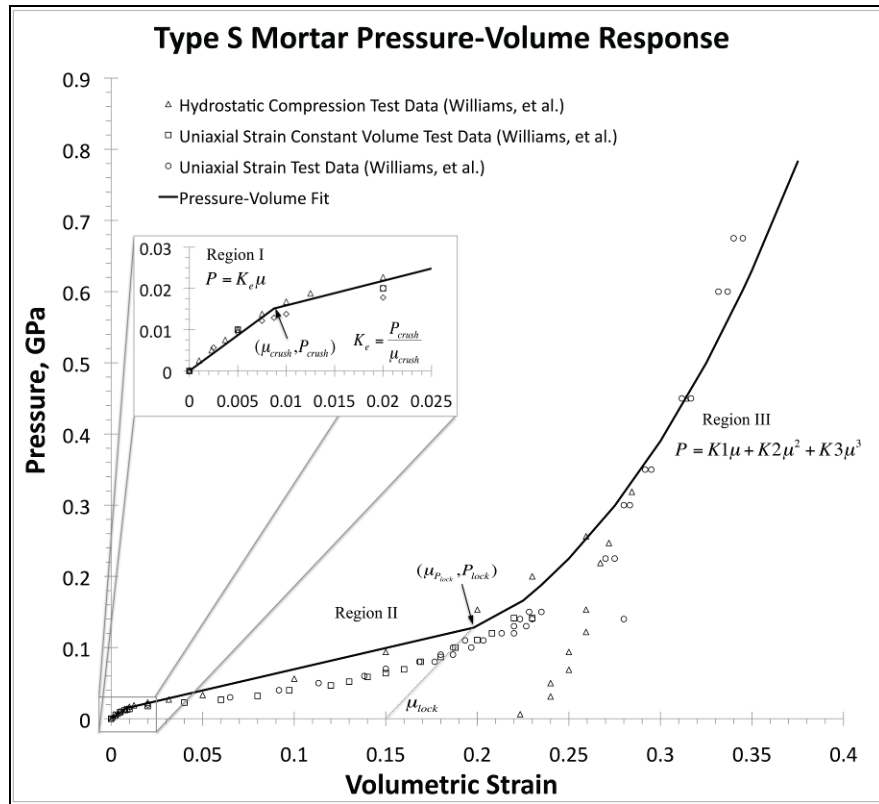
Pressure, GPa

Volumetric Strain

Figure 5. HJC material model pressure-volume fit for type S mortar.

6

Region II begins and the linear elastic behavior governing Region I ends with parameters P_{crush} and μ_{crush}, which are the pressure and volumetric strain at which the material begins to undergo plastic deformation. Permanent, plastic deformation in brittle geomaterials, which are riddled with tiny pores and air voids, may be described as micro-cracking and air void crushing as pressure and volumetric strain increase beyond P_{crush} and μ_{crush}. Fracture and void collapse occur in Region II, shown in figures 4 and 5. Holmquist et al. (*1*) define Region II as a transition region; the model interpolates the material behavior in this region between Regions I and III. The user of the model cannot directly control the predicted material behavior in this region other than by controlling the model parameters that govern behavior for Regions I and III.

The onset of Region III, shown in figures 4 and 5, is controlled by the parameters P_{lock} and μ_{lock}, which are the pressure and volumetric strain at which all air voids have been crushed out of the material. P_{lock} and μ_{lock} were determined by fitting to HC and UX data. Holmquist et al. (*1*) describe Region III as the behavior for fully dense material, where all air voids have been crushed out of the material. In this region the material is locked and cannot compress any farther in either plastic deformation or void collapse. However, since the material is under hydrostatic compression and the volume of material has nowhere to go, the pressure begins to increase dramatically for very small changes in volumetric strain. The material behavior in this region is governed by equation 4, which is a fit between high-pressure hydrostatic compression data and shock Hugoniot data (*13*). In equation 4, pressure is a function of volumetric strain, μ, and three constants, *K1*, *K2*, and *K3* are used to fit a cubic equation to the data as seen in figures 4 and 5. The use of modified volumetric strain described by Holmquist et al. (*1*) shifts the high-pressure region back to the origin so that there is no apparent softening due to void collapse under very high pressure stimuli.

$$P = K1\mu + K2\mu^2 + K3\mu^3 \tag{4}$$

Shock Hugoniot data from Los Alamos National Laboratory (*13*) used for the type S mortar high-pressure fit was from gas shale with an average initial density of 2.54761 g/cm^3, which most closely matched the type S mortar grain (or fully consolidated) density of 2.510 g/cm^3. Shock Hugoniot data used for the grade SW brick high-pressure fit was from fused quartz with an average initial density of 2.204 g/cm^3, which most closely matched the grade SW brick grain density of 2.250 g/cm^3. At the extremely high pressures of the shock Hugoniot data, inertial effects, rather than strength effects, dominate the material behavior; thus, at these pressures, it is assumed that matching the density is more important than matching the composition or strength of the material. Since shock Hugoniot data was not available for brick or mortar, using materials that somewhat resemble the geomaterials is assumed to be acceptable if the density is closely matched; this assumption only affects the constants for equation 4 and the high-pressure behavior of the material.

3.   Numerical Simulations with Material Parameters

Numerical simulations using the material parameters for brick and mortar were compared with true stress and engineering strain data provided by ERDC (*8, 9*). The shock physics code CTH (*12*) was used to stress a 1-cm^3 cube with 10 uniformly distributed cells per side. Use of a flow code such as CTH is not ideal for simple deformation induced stress and strain, but time constraints necessitated the use of CTH as a near-term solution as it has the HJC model readily available and the model had been in use for geomaterial simulations. Future work is expected to use the EPIC code to test material parameters. However, CTH provided an acceptable first look at the efficacy of the material parameters.

The material parameters for grade SW brick and type S mortar were applied to the cube and strain was applied to the cube using the prescribed deformation (PRDEF) utility in CTH (*12*). Three different mechanical tests were simulated by applying strain to the cube to produce compression against set boundary conditions. Strain was applied in different configurations of the three directions to produce the following loading scenarios: (1) uniaxial compression—strain was applied axially while the radial directions were confined, (2) hydrostatic compression—strain was applied equally in all three directions, and (3) triaxial compression—strain was applied in hydrostatic compression to a set level, in this case, 200 MPa, and then held constant while the axial strain was increased to failure. Failure strains were determined from mechanical test data.

Figures 6 and 7 show the results of low-pressure uniaxial simulations compared with ERDC test data by Williams et al. for grade SW brick (*8*) and type S mortar (*9*), respectively. Figures 8 and 9 show the results of hydrostatic simulations compared with ERDC test data by Williams et al. for grade SW brick (*8*) and type S mortar (*9*), respectively. Figures 10 and 11 show the results of triaxial compression simulations compared with ERDC test data by Williams et al. for grade SW brick (*8*) and type S mortar (*9*), respectively. Additionally, uniaxial simulations were strained to extremely high pressures indicative of penetration events; however, high-pressure test data were only available for grade SW brick (*14*). Figure 12 shows the result of the high-pressure uniaxial simulation for grade SW brick.
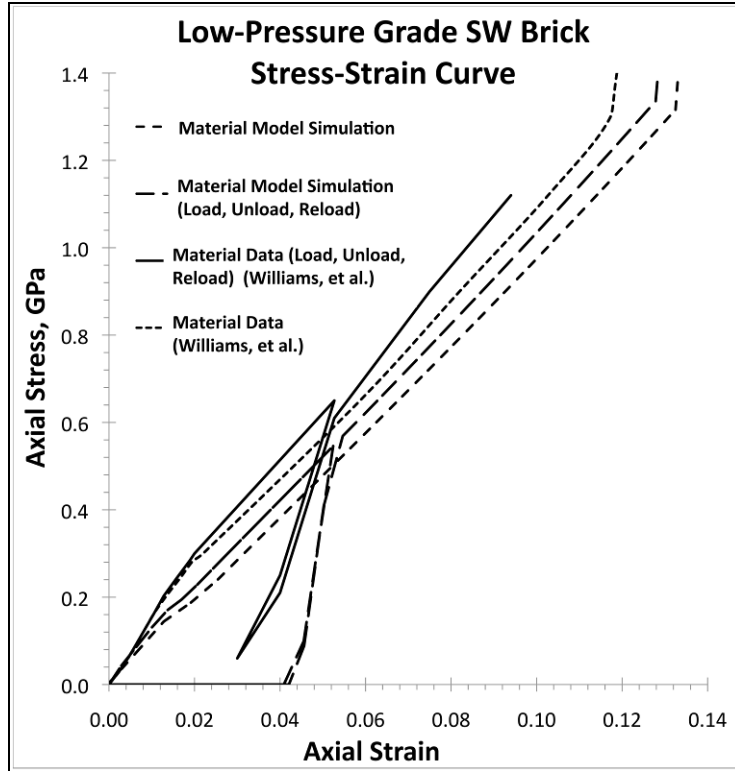
Figure 6. Uniaxial strain test data compared with simulation results
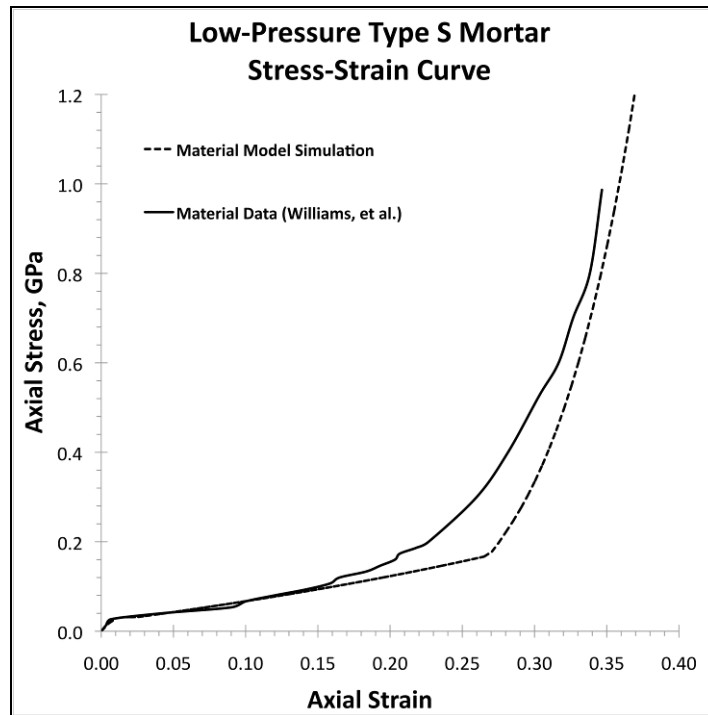for grade SW brick.

Figure 7. Uniaxial strain test data compared with simulation results
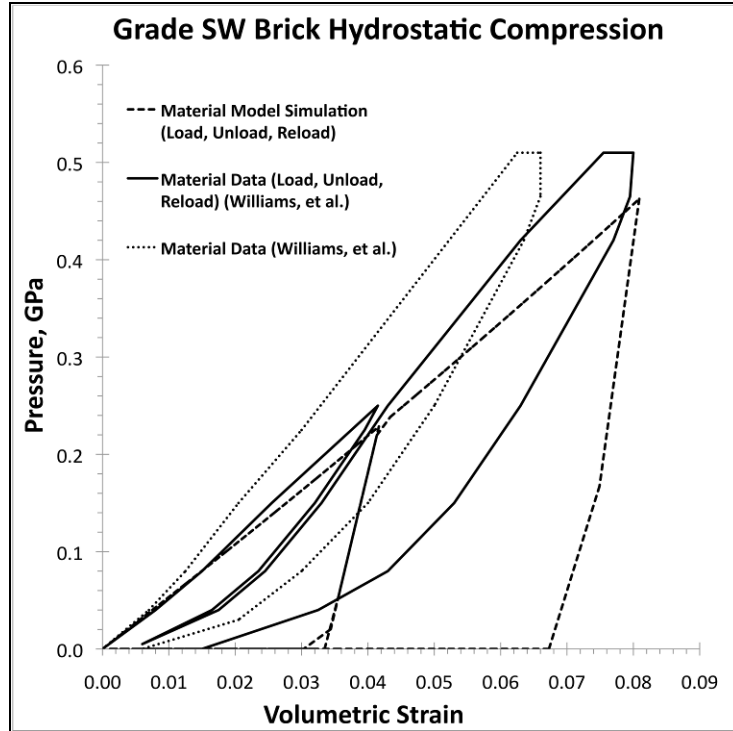for type S mortar.

Figure 8. Hydrostatic compression test data compared with simulation
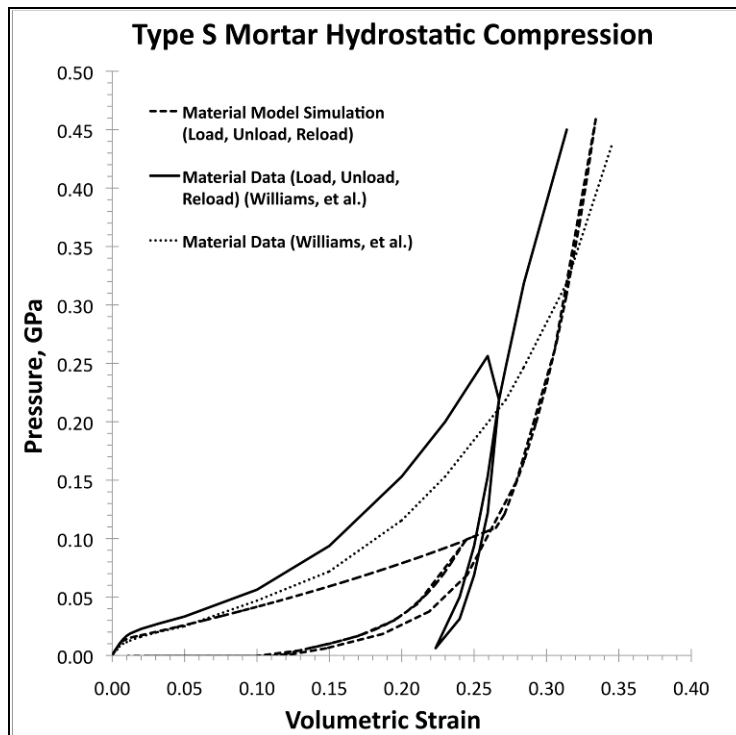results for grade SW brick.

Figure 9. Hydrostatic compression test data compared with simulation
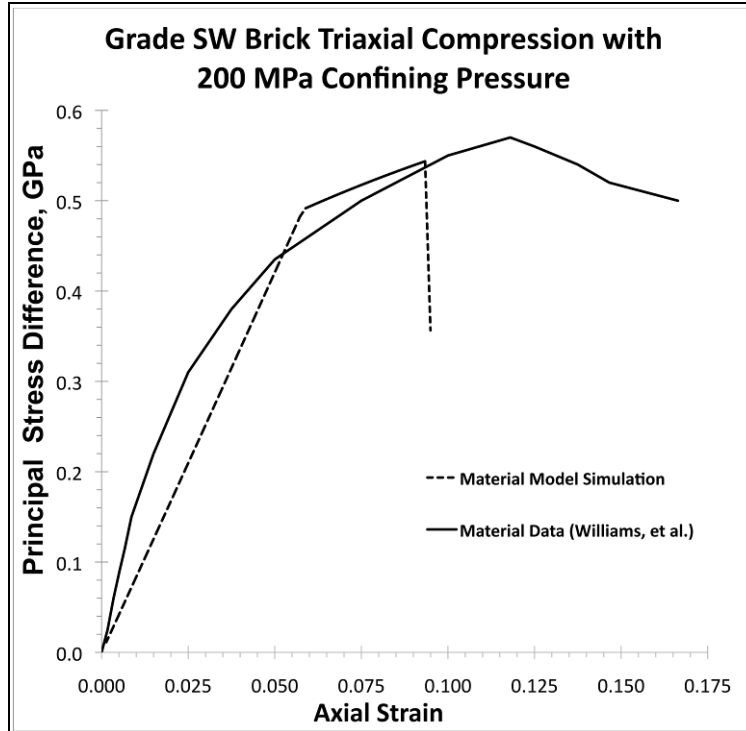results for type S mortar.

Figure 10. Triaxial compression test data compared with simulation results for grade SW brick.
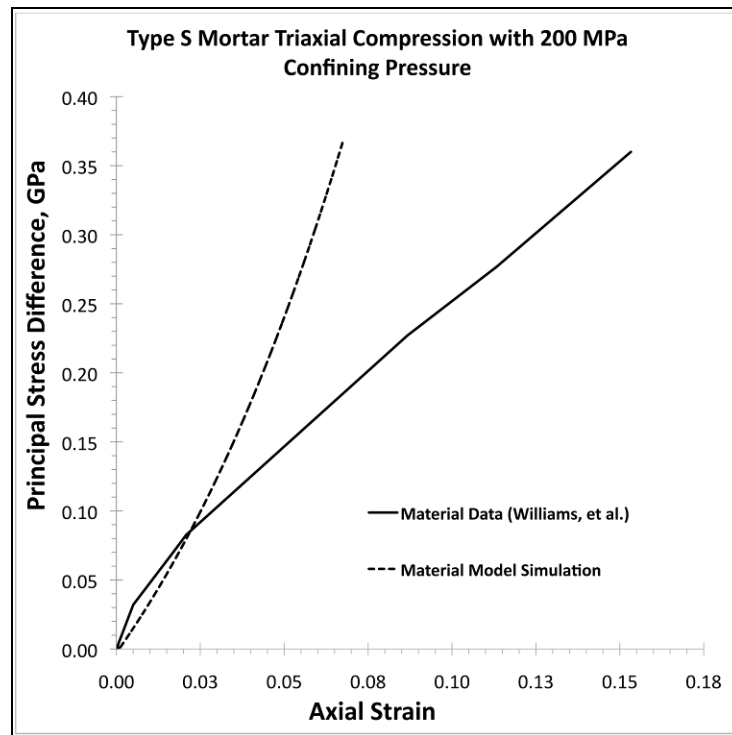

Figure 11. Triaxial compression test data compared with simulation results for type S mortar.
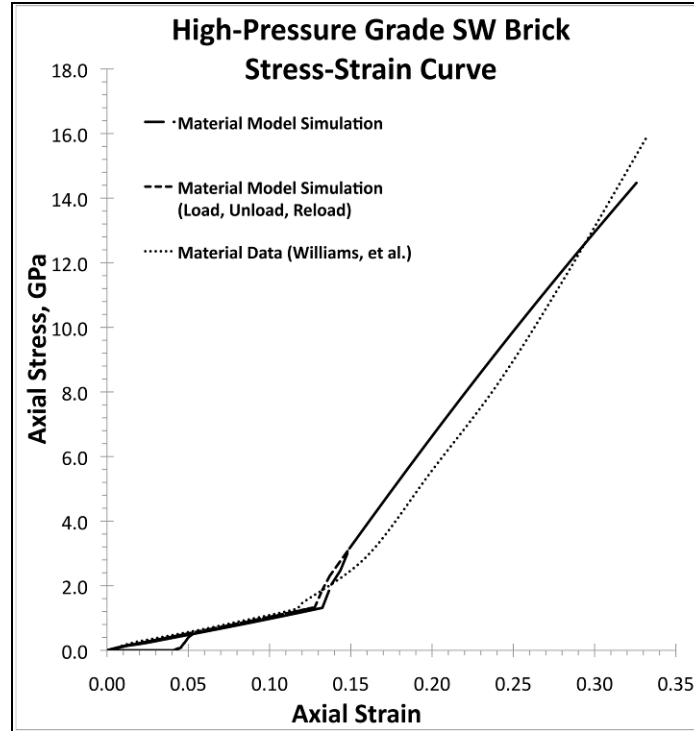
Figure 12. High-pressure uniaxial strain test data compared with
simulation results for grade SW brick.

4. Summary and Conclusions

Table 1 contains the HJC constitutive model (*1*) material parameters for grade SW brick and type S mortar. Sample numerical simulations were performed to compare the model parameters to mechanical test data (*8, 9*). Simulations included uniaxial compression, hydrostatic compression, and triaxial compression loading scenarios. Although the HJC model has been reported to overpredict the penetration rate for high velocity impacts into concrete and miss the wide variation in entry and exit hole size, it was also reported to predict residual velocity fairly well (*7*). The HJC model remains one of a limited number of tools available for use in hydrocode simulations of geomaterials (*12*). Since the use of an Eulerian code such as CTH is not ideal for simulations of simple strain induced deformations, additional simulations in EPIC will be used in the future for further examination of these parameters. However, the CTH code does provide the PRDEF subroutine (*12*) for use in examining the behavior of material models in CTH simulations, and the results of the sample numerical simulations conducted here predict stress-strain behavior reasonably well when compared with mechanical characterization test data. Sample numerical simulations were limited in scope due to time constraints and did not explore damage; further study of the damage behavior of these materials is desirable to understand the effect of fracture on material strength. Penetration experiments would provide the high-pressure

12

and fracture data needed for comparing simulations of penetrations using these material parameters to penetration events; these parameters will be further explored if such data becomes available. Development of constitutive material models for brick and for mortar for use in high-velocity penetration simulations is ideal but impractical; these material parameters provide a near-term solution for modeling brick and mortar masonry in penetration simulations.

Table 1. HJC constitutive model material parameters for brick and mortar.

Property		Unit	Grade SW Brick	Type S Mortar	Type N Mortar	Adobe
Initial density[a]	ρ_o	kg/m^3	1986	1604	1554	1599
Grain density[a]	ρ_{grain}	kg/m^3	2250	2510	2510	2510
Sound speed[a]	C_s	cm/s	2.56E+05	2.52E+05	2.04E+05	1.4425E+05
Cohesive strength coefficient	A		0.63646	0.66	0.652778	0.435255
Pressure hardening coefficient	B		1.568	1.335	1.079	1.27
Pressure hardening exponent	N		0.8264	0.845	0.835	0.857
Strain rate coefficient	C		0.0054	0.0018	0.0023	0.0023
Compressive strength	f'c	GPa	0.075	0.0123	0.00485	0.003118
Tensile strength	T	GPa	0.006	0.0018	0.0008375	0.000112
Maximum strength	SMAX		17.33	80.24	213	137.9
Shear modulus[a]	G	GPa	5.18	1.15	0.51	0.209
Bulk modulus[a]	K	GPa	5.3	1.7	0.71	0.318
Damage constant 1	D1		0.01413	0.006629	0.0102632	0.017758
Damage constant 2	D2		1.0	1.0	1.0	1.0
Minimum fracture strain	EFMIN		0.01	0.01	0.01	0.01
Crush pressure	P_{crush}	GPa	0.03519	0.0138	0.05833	0.00096
Crush volumetric strain	μ_{crush}		0.00664	0.0075	0.2	0.003
Pressure constant 1	K1	GPa	63	0.3	12.436	0.45
Pressure constant 2	K2	GPa	-79	-2	-49.003	-3.9879
Pressure constant 3	K3	GPa	56	19	69.424	19.766
Lock pressure	P_{lock}	GPa	0.773	0.1096	0.23167	0.022607
Lock volumetric strain	μ_{lock}		0.132931	0.15	0.33	0.09

[a]Reported in Williams et al. (*8, 9*).

5. References

1. Holmquist, T. J.; Johnson, G. R.; Cook, W. H. A Computational Constitutive Model For Concrete Subjected To Large Strains, High Strain Rates, and High Pressures. *Intl Symp on Ballistics* **1993**, *14*, 591–600.

2. Wei, X.; Hao, H. Numerical Derivation of Homogenized Dynamic Masonry Material Properties with Strain Rate Effects. *International Journal of Impact Engineering* **2009**, *36*, 522–536.

3. Zucchini, A.; Lourenço, P. B. Mechanics of Masonry in Compression: Results from a Homogenization Approach. *Computers and Structures* **2007**, *85*, 193–204.

4. Wei, X.; Stewart, M. G. Model Validation and Parametric Study on the Blast Response of Unreinforced Brick Masonry Walls. *Intl J Impact Engineering* **2010**, *37*, 1150–1159.

5. Wang, M.; Hao, H.; Ding, Y.; Li, Z. Prediction of Fragment Size and Ejection Distance of Masonry Wall Under Blast Load Using Homogenized Masonry Material Properties. *Intl J Impact Engineering* **2009**, *36*, 808–820.

6. Shieh-Beygi, B.; Pietruszczak, S. Numerical analysis of structural masonry: mesoscale approach. *Computers and Structures* **2008**, *86*, 1958–1973.

7. Dawson, A.; Bless, S.; Levinson, S.; Pedersen, B.; Satapathy, S. Hypervelocity Penetration of Concrete. *Intl J Impact Engineering* **2008**, *35*, 1484–1489.

8. Williams, E. M.; Akers, S. A.; Reed, P. A. *Laboratory Characterization of Solid Grade SW Brick*; Geotechnical and Structures Lab Tech. Rep., ERDC/GSL TR-07-24, 2007.

9. Williams, E. M.; Akers, S. A.; Reed, P. A. *Laboratory Characterization of Type S Mortar*; Geotechnical and Structures Lab Tech. Rep., ERDC/GSL TR-08-10, 2008.

10. Hao, H.; Tarasov, B. G. Experimental Study of Dynamic Material Properties of Clay Brick and Mortar at Different Strain Rates. *Australian Journal of Structural Engineering* **2008**, *8* (2), 117–131.

11. Grote D. L.; Park, S. W.; Zhou, M. Dynamic Behavior of Concrete at High Strain Rates and Pressures: I. Experimental Characterization. *Intl. J. Impact Engineering* **2001**, *25*, 869–886.

12. Crawford, D. A., ed. *CTH User's Manual and Input Instructions, Version 8.1*; Sandia National Laboratories, pp 115–118, 2007.

13. Marsh, S. P., ed. *LASL Shock Hugoniot Data*, University of California Press, 1980.

14. Akers, S.; Adley, M. Private communication. 31 March 2009.

List of Symbols, Abbreviations, and Acronyms

DIF   dynamic increase factors

ERDC   Engineer Research and Development Center

HC   hydrostatic compression

HJC   Holmquist-Johnson-Cook

PRDEF   prescribed deformation

TXC   triaxial compression

UX   uniaxial strain

ABERDEEN PROVING GROUND

44   DIR USARL
     RDRL CIH C
        J CAZAMIAS
     RDRL SLB W
        W BRUCHEY
     RDRL WML
        D LYON
        J NEWILL
     RDRL WML H
        C CANDLAND
        T EHLERS
        T FARRAND
        M FERMEN-COKER
        E KENNEDY
        L MAGNESS
        C MEYER
        R PHILLABAUM
        D SCHEFFLER
        S SCHRAML
        B SCHUSTER
        B SORENSEN
        R SUMMERS
     RDRL WMP B
        R BECKER
        S BILYK
        D CASEM
        J CLAYTON
        J HOUSKAMP
        R KRAFT
        B LEAVY
        B LOVE
        M RAFTENBERG
        T WEERISOORIYA
        C WILLIAMS

     RDRL WMP C
        T BJERKE
        N BRUCHEY
        S SEGLETES
        W WALTERS
     RDRL WMP D
        R DONEY
        D KLEPONIS
        H MEYER
        F MURPHY
        B VONK
        G VUNNI
        M ZELLNER
     RDRL WMP E
        B CHAMISH
        M LOVE
        C NICELY
     RDRL WMP G
        R BANTON
        S KUKUCK

TOTAL: 75 (1 ELEC, 74 HCS)

INTENTIONALLY LEFT BLANK.